Pharmacological Reports (2020) 72:1433–1440
https://doi.org/10.1007/s43440-020-00124-z

SHORT COMMUNICATION

Radiosynthesis and evaluation of [^{18}F]FMTP, a COX-2 PET ligand

J. S. Dileep Kumar[1] · Jaya Prabhakaran[1,2] · Andrei Molotkov[3] · Anirudh Sattiraju[3] · Jongho Kim[3] · Mikhail Doubrovin[3] · J. John Mann[1,2,3] · Akiva Mintz[3]

Received: 6 April 2020 / Revised: 22 June 2020 / Accepted: 25 June 2020 / Published online: 6 July 2020

Abstract

Background The upregulation of cyclooxygenase-2 (COX-2) is involved in neuroinflammation associated with many neurological diseases as well as cancers of the brain. Outside the brain, inflammation and COX-2 induction contribute to the pathogenesis of pain, arthritis, acute allograft rejection, and in response to infections, tumors, autoimmune disorders, and injuries. Herein, we report the radiochemical synthesis and evaluation of [^{18}F]6-fluoro-2-(4-(methylsulfonyl)phenyl)-*N*-(thiophen-2-ylmethyl)pyrimidin-4-amine ([^{18}F]FMTP), a high-affinity COX-2 inhibitor, by cell uptake and PET imaging studies.

Methods The radiochemical synthesis of [^{18}F]FMTP was optimized using chlorine to fluorine displacement method, by reacting [^{18}F]fluoride/K222/K_2CO_3 with the precursor molecule. Cellular uptake studies of [^{18}F]FMTP was performed in COX-2 positive BxPC3 and COX-2 negative PANC-1 cell lines with unlabeled FMTP as well as celecoxib to define specific binding agents. Dynamic microPET image acquisitionwas performed in anesthetized nude mice ($n=3$), lipopolysaccharide (LPS) induced neuroinflammation mice ($n=4$), and phosphate-buffered saline (PBS) administered control mice ($n=4$) using a Trifoil microPET/CT for a scan period of 60 min.

Results A twofold higher binding of [^{18}F]FMTP was found in COX-2 positive BxPC3 cells compared with COX-2 negative PANC-1 cells. The radioligand did not show specific binding to COX-2 negative PANC-1 cells. MicroPET imaging in wild-type mice indicated blood–brain barrier (BBB) penetration and fast washout of [^{18}F]FMTP in the brain, likely due to the low constitutive COX-2 expression in the normal brain. In contrast, a ~ twofold higher uptake of the radioligand was found in LPS-induced mice brain than PBS treated control mice.

Conclusions Specific binding to COX-2 in BxPC3 cell lines, BBB permeability, and increased brain uptake in neuroinflammation mice qualifies [^{18}F]FMTP as a potential PET tracer for studying inflammation.

Keywords PET · COX-2 · Radiotracer · Inflammation · Brain

Abbreviations

AD	Alzheimer's disease;
ALS	Amyotrophic lateral sclerosis;
BBB	Blood–brain barrier;
CNS	Central nervous system;
COX2	Cyclooxigenase-2;
COXIBs	COX-2 inhibitors;
LPS	Lipopolysaccharide;
NSAID	Non-steroidal anti-inflammatory drugs;
MDD	Major depressive disorders;
PBS	Phosphate-buffered saline;
PD	Parkinson's disease;
PET	Positron Emission Tomography;
RCY	Radiochemical yield;
SUVs	Standardized uptake values;
TACs	Time-activity curves;
TBAF	Tetra-n-butyl ammonium fluoride;
TBI	Traumatic brain injury;
VOI	Volume of interest

✉ J. S. Dileep Kumar
Dileep.Kumar@nyspi.columbia.edu

✉ Akiva Mintz
am4754@cumc.columbia.edu

[1] Molecular Imaging and Neuropathology Division, New York State Psychiatric Institute, Manhattan, NY, USA

[2] Department of Psychiatry, Columbia University Medical Center, Manhattan, NY, USA

[3] Department of Radiology, Columbia University Medical Center, Manhattan, NY, USA

Introduction

Cyclooxygenase (COX) or prostaglandin endoperoxidase synthase, is an enzyme involved in the biosynthesis of prostaglandins, prostacyclins and thromboxanes from arachidonic acid [1–3] Among the three known isoforms of COX (COX-1, COX-2 and COX-3), COX-1 has predominantly constitutive activity and is involved in many normal physiological functions [1–3]. In contrast, COX-2 is inducible, with relatively low constitutive activity and mostly found in kidney, brain, and heart [1–6]. The third isoform, COX-3, may be responsible for febrile response and mediates the antipyretic effects of aspirin and acetaminophen. COX-2 inhibition mediates the analgesic activities of nonsteroidal anti-inflammatory medications (NSAIDs) [7–9]. COX-2, induced by inflammatory stimuli, catalyzes prostanoid formation associated with inflammation and proliferative diseases.1–3 In the central nervous system (CNS). Neuroinflammation and COX-2 induction are implicated in the pathogenesis of neurodegenerative diseases such as Alzheimer's disease (AD), Parkinson's disease (PD), amyotrophic lateral sclerosis (ALS), as well as psychiatric disorders, smoking, seizure disorders, and traumatic brain injury (TBI) [10–15]. COX-2 induction is also involved in pain, arthritis, cancers, myocardial infarction, and acute allograft rejection [5, 16–21]. COX-2 inhibitors (COXIBs) have anti-inflammatory effects [22–24].

Monitoring in vivo changes in COX-2 expression allows quantification of inflammation, tracking of disease course, and assessing target occupancy of newly developed NSAIDs and or monitoring clinical use of FDA-approved COXIB medications. At present, COX-2 quantification is accomplished by ex vivo assays of tissue samples, invasively obtained from biopsies. PET imaging would allow non-invasive and in vivo visualization of COX-2 throughout the body. Existing COX-2 PET ligands are not successful for in vivo quantification of COX-2 due to limitations such as suboptimal COX-2 affinity, high nonspecific binding, de^{18}F-fluorination, and skeletal uptake, poor brain or organ uptake, inability to detect basal or low level of COX-2, and poor signal to noise ratio due to lipophilicity [25–35].[^{11}C]TMI, a highly potent COX-2 inhibitor, developed by our group is the only radiotracer exhibiting partial blocking of constitutive COX-2 level in baboon brain, however, its ability to image inflammation in animal disease models is yet to be proven [36]. A recent report demonstrates that [^{18}F]pyricoxib, a COX-2 inhibitor belonging to the class of 2-(4-methylsulfonylphenyl)lpyrimidines, and triazole analog [^{18}F]triacoxib showed a higher binding in COX-2 positive cells (HCA-7) compared with COX-2 negative cells (HCT-116). However, both tracers demonstrated only modest binding in xenografts, in vivo and did not show significant uptake in the brain (Fig. 1) [37–39]. Similarly, [^{11}C]MC1, another member of the class of arylpyrimidines, showed increased binding to COX-2 in animal models of neuroinflammation (Fig. 1) [40]. Despite promising uptake in neuroinflammation, [^{11}C] MC1 failed to detect constitutive or low level of COX-2 in the brain under conditions without inflammation and cold MC1 confirmed no specific binding in CNS and periphery organs [41]. We posit that COX-2 selective inhibitors with sub-nanomolar affinity and radiolabeled with long-lived isotopes such as 18-F (decay half-life 110 min) may help to overcome some of the limitations of the known tracers. Hence, herein, we report the radiosynthesis and evaluation of [^{18}F]6-fluoro-2-(4-(methylsulfonyl)phenyl)-N-(thioph-en-2-ylmethyl) pyrimidin-4-amine ([^{18}F] FMTP; COX-2 $IC_{50} = 2.5$ nM), as potential PET ligand for COX-2 imaging in brain and periphery (Fig. 1) [42, 43]. The synthesis of unlabeled FMTP was reported by reacting thiophen-2-ylmethanamine with 4,6-difluoro-2-(4-(methylsulfonylphenyl) pyrimidine [44]. We choose [^{18}F]FMTP, belonging to the pyrimidine class of COX-2 inhibitors, as a potential PET tracer for COX-2 imaging owing to the presence of a chemically and metabolically stable radiolabeling position on the aromatic ring, level of lipophilicity for passive brain entry, and high COX-2 affinity and high selectivity index of COX-1/COX-2 of the pyrimidine-based class of COX-2 inhibitors having the FMTP structure [44, 45].

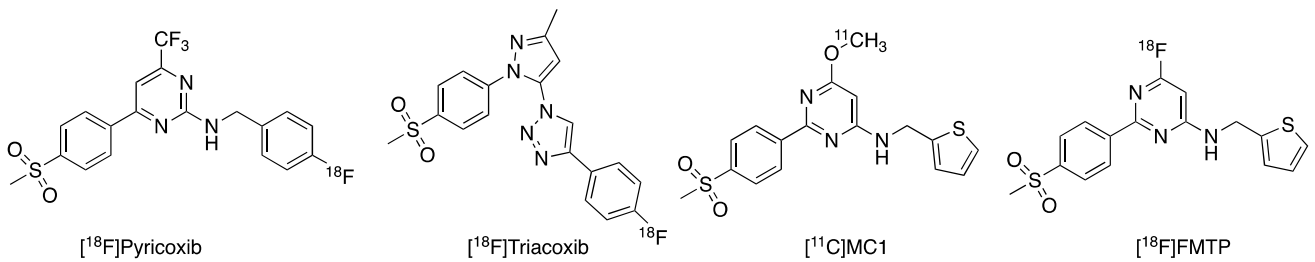

Fig. 1 Chemical structures of [^{11}C]MCI, [^{18}F]Pyricoxib, [^{18}F]Triacoxib and [^{18}F]FMTP

Materials and methods

All commercial chemicals and solvents used in the synthesis were purchased from Sigma-Aldrich Chemical Co. (St. Louis, MO), or Fisher Scientific Inc. (Springfield, NJ) and were used without further purification. 18F-fluoride was produced using RDS112 cyclotron (Siemens, Knoxville, TN). Gamma-ray detector (Bioscan Flow-Count fitted with a NaI detector) coupled in series with the UV detector (Waters Model 996 set at λ 254 nm) was used for detection of radiolabeled products. Data acquisition for both the analytical and preparative systems was accomplished using a Waters Empower Chromatography System. BxPC3 and PANC1 pancreas carcinoma human cell lines were obtained from ATCC (Manassas, VA). Dynamic microPET image acquisitions were performed with Trifoil microPET/CT scanner.

Synthesis of Cl-MTP

Thiophen-2-ylmethanamine (68 mg, 0.6 mmol) was added to a solution of 4,6-dichloro-2-(4-(methylsulfonyl)phenyl) pyrimidine (0.3 mmol, 90 mg) in 4 mL dry dichloromethane and 0.1 mL triethylamine. The reaction mixture was stirred at room temperature for 1 h and at this time, HPLC analyses showed > 95% consumption of the chloro-substrate. The reaction mixture was evaporated and chromatographed over silica gel using 40:60 ethylacetate-hexane to afford 75 mg (65%) of Cl-MTP as pale yellow solid.

Cl-MTP: mp: 169–171 °C [42, 43, 45]; ^{1}H NMR (400 MHz, $CDCl_3$): 3.0 (3H, s, CH_3), 4.85 (2H, bs, CH_2), 5.3 (1H, bs, NH), 6.3 (1H,s), 6.9 (1H, m), 7.0 (1H,d, J = 2.81 Hz), 7.2 (2H, d, overlapped with $CDCl_3$), 7.9 (2H, d, J = 8.53 Hz),8.5 (2H,d, J = 8.56 Hz).

Synthesis of fluoro-MTP

Tetra-n-butyl ammonium fluoride (TBAF) (0.1 mL, 1 M solution in. THF) was added to a solution of Cl-MTP (20 mg, 0.05 mmol) in DMF (2 mL). The resulting solution was heated at 140 °C for 1 h at which time point, HPLC analyses showed > 95% consumption of Cl-MTP. The reaction mixture was then allowed to cool, diluted with water (20 mL), and extracted with ethyl acetate (3 × 10 mL). The combined ethyl acetate fractions were further washed with saturated brine, dried over anhydrous $MgSO_4$ and chromatographed over silica gel (20:80 ethyl acetate-hexane) to afford 15 mg (85%) of FMTP as pale yellow solid. The analytical data of F-FMTP is in agreement with the reported data [44].

FMTP: m.p: 131.5 °C; ^{1}H NMR (400 MHz, $CDCl_3$): δ 3.0 (3H, s, CH_3), 4.8 (2H, bs, CH_2), 5.9 (1H, bs, NH), 6.4 (1H, s), 6.9–7 (1H, m), 7.05 (1H, d, J = 2.82 Hz), 7.2 (2H, d, overlapped with $CDCl_3$), 8 (2H, d, J = 8.51), 8.6 (2H,d, J = 8.54); HRMS (MH^+) calculated for: $C_{16}H_{15}FN_3O_2S_2$: 364.0512; Found: 364.0533.

Radiosynthesis of [^{18}F]FMTP

18F-fluoride (Eclipse cyclotron, Siemens) trapped from QMA was eluted with 1 mL of 10:1 acetonitrile: water, containing kryptofix K222 (36 mg) and potassium carbonate (2 mg). The reaction mixture was azeotropically heated and dried at 98 ºC under a stream of argon by the repeated addition of acetonitrile (4 × 0.5 mL). A solution of ~ 2 mg of Cl-MTP in 500 µL of DMSO was then added to the reaction vial, sealed, and heated for 20 min at 140 ºC. The reaction mixture was allowed to cool to room temperature and diluted with 20 mL water and passed through a classic C-18 Sep-Pak cartridge and eluted with 1 mL acetonitrile. The crude product in acetonitrile was injected onto a semi-preparative HPLC column (Phenomenex, Prodigy ODS-Prep 10 × 250 mm, 10 µ; and eluted with 50:50 acetonitrile-0.1 M ammonium formate with a flow rate of 8 mL/min).[^{18}F]FMTP eluted at 9–10 min was collected based on the γ-detector reading, diluted with 50 mL of deionized water, and passed through a classic C-18 Sep-Pak cartridge, washed with 10 mL of deionized water and eluted with 1 mL of ethanol. Reconstruction of the product in 1 mL of absolute ethanol afforded [^{18}F]FMTP in 35 ± 5% yield (EOS). A portion of the ethanol solution was analyzed by analytical HPLC (Phenomenex, Prodigy ODS(3) 4.6 × 250 mm, 5 µ; mobile phase; 60:40 acetonitrile-0.1 M AMF, flow rate 2 mL/min, tR = ~ 5 min) to determine the specific activity, chemical and radiochemical purities. The ethanol solution was then diluted to a volume of 10 ml with saline and filtered through a sterile environment, and a portion of this solution was formulated for injection.

Cell uptake of [^{18}F]FMTP.

BxPC3 and Panc1 pancreas carcinoma human cell lines were plated on a 24-well plate at 2 × 105 cells/well. After 48 h, [^{18}F]FMTP was added (2.0 µCi/mL) to the cell medium for 30 min. For blocking experiments, non-labelled FMTP or celecoxib (5 M) was added to cells 30 min before [^{18}F] FMTP. After incubation with [^{18}F]FMTP cells were washed 4 times with cold PBS, lysed with 0.1 N NaOH, and counted in a gamma counter (Hidex AMG, LabLogic, Tampa, FL).

Micro PET imaging

The animals (male white mice) were anesthetized with isoflurane (1–2% isoflurane in 100% oxygen) using a nose cone, and a 29-gauge needle connected to a catheter was placed into the lateral tail vein ($n = 3$). For neuroinflammation, mice

were stereotactically injected with 5 µg of LPS or PBS (controls) in the brain, adopting a known procedure [46, 47], and waited 24 h for imaging experiments ($n = 4$). The animal was placed in a prone position on the platform of the scanner and moved into the center of the field of view guided by laser beam calibration. Immediately after scan start, [^{18}F]FMTP (~2.5 MBq 25 mL in 20% ethanol-saline solution) was injected through the tail-vein catheter manually. The error caused by the injector and catheter was corrected by subtracting the remaining dose. 40 min dynamic imaging was acquired on a microPET scanner (Siemens Inveon). The acquired list-mode data were reconstructed with 3-D ordered subset expectation maximization (OSEM) algorithm [48, 49] using the software of Siemens Inveon Acquisition Workplace with a framing protocol of 2 × 30 s, 4 × 60 s, 3 × 120 s, 3 × 180 s, and 4 × 300 s.

PET data analysis

Using PMOD software (version 4.0, Switzerland), the three-dimensional ellipsoid volume of interests (VOIs) ranging from 2-to-6 mm were placed manually at the center of the brain, heart (blood-pool), liver, proximal humerus (bone) and posterior cervical muscle. The standardized uptake values (SUVs) were estimated using a calibration factor calculated from the phantom study and time-activity curves (TACs) were derived from VOIs in the series of reconstructed images.

Results and discussion

Synthesis of FMTP and radiosynthesis of [^{18}F]FMTP

Synthesis of Cl-MTP, the radiolabeling precursor molecule, was achieved in four steps from commercially available 4-(methylthio)benzimidamide in 65% yield by adopting a previously reported procedure (Scheme 1) [45]. The non-radioactive standard FMTP was obtained in 85% yield by reacting Cl-MTP with TBAF in dimethyl sulfoxide (DMSO) as shown in Scheme 1. Our approach for the synthesis of FMTP was different than previously reported [43]. The radiosynthesis of [^{18}F]FMTP was optimized by reacting 18F-fluoride/K_{222}/K_2CO_3 using chlorine to 18F-fluorine displacement reaction with the precursor molecule (Scheme 1). To our knowledge, this is the first successful radiolabeling of a chlorine to-18F-fluorine displacement at the 6th position of aryl[1,3]pyrimidines.[^{18}F]FMTP was obtained in 35 ± 5% yield at EOS with > 99% radiochemical purity and a molar activity of 92.5 ± 18.5 GBq/µ mol ($n = 10$). The total synthesis time of [^{18}F]FMTP was 1 h at EOS and the radioligand was found to be stable in 10%-ethanol-saline formulation.

Cell uptake of [^{18}F]FMTP

After the successful radiosynthesis and formulation, proof of concept and selectivity of [^{18}F]FMTP binding to COX-2

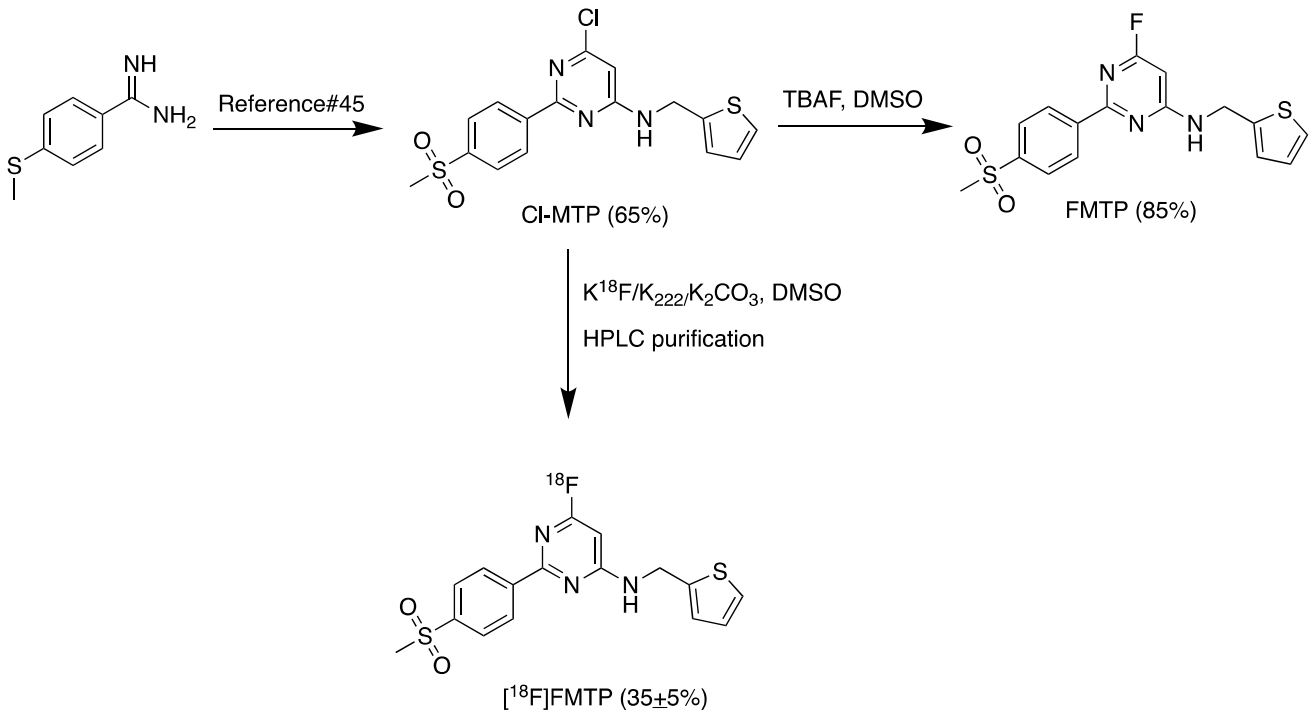

Scheme 1 Synthesis of FMTP and radiosynthesis of [^{18}F]FMTP

was examined by evaluating the tracer uptake in COX-2 positive BxPC3 and a control COX-2 negative PANC1 human pancreatic carcinoma cell lines. Figure 2 illustrates a > twofold uptake of [18F]FMTP in BxPC3 cells compared with PANC1 cells. This binding was substantially blocked with unlabeled FMTP. Blocking with celecoxib, an FDA approved COX-2 inhibitor, produced less proportional blocking compared with cold FMTP. As anticipated [18F]FMTP showed negligible binding to PANC1 cells and no specific binding with FMTP or celecoxib block.

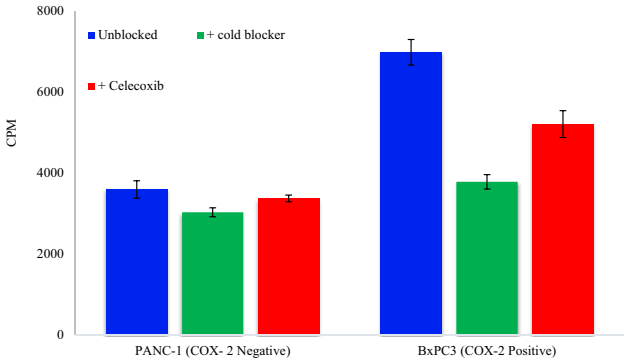

Fig. 2 Binding of [18F]FMTP in BxPC3 and PANC-1 cells. Values are reported as the mean ± SD from four independent experiments

MicroPET evaluation of [18F]FMTP

MicroPET evaluation of [18F]FMTP was initially performed in nude white mice ($n = 3$). Figure 3 shows the summed early frames (0–10 min) and total frames (0–40 min) of microPET images. As evident from the images, the tracer penetrates the BBB and subsequently shows a fast washout of activity from the brain. Time activity curves (TACs) also indicate an initial rapid influx of radioactivity followed by rapid washout (Fig. 4). The uptake of [18F]FMTP peaked around one minute in heart and brain and then decreases rapidly. The absence of retention of [18F]FMTP activity in these organs is predicted due to low COX-2 expression in the normal mouse brain. The highest radioactivity outside the heart was found in the liver, and the delay to peak at 5–10 min is probably due to the accumulation of radioactive metabolite(s). The tracer did not show uptake in the spine and skeleton which indicates a lack of de18F-fluorination, an advantage of [18F]FMTP for use in in vivo PET imaging. We studied the binding of [18F]FMTP in LPS-induced neuroinflammation in mice compared with vehicle (PBS) treated-mice [46]. Intracranial injection of LPS in mice is known to generate COX-2 induction and neuroinflammation after around 24 h [47]. Therefore, we performed PET imaging of LPS treated mice after 24 h with [18F]FMTP and found an approximately twofold increase of tracer binding in the brain compared with PBS-treated mice ($n = 4$) (Fig. 5). TACs in whole-brain confirmed higher binding of [18F]FMTP in LPS treated mice compared with PBS treated controls (Fig. 6).

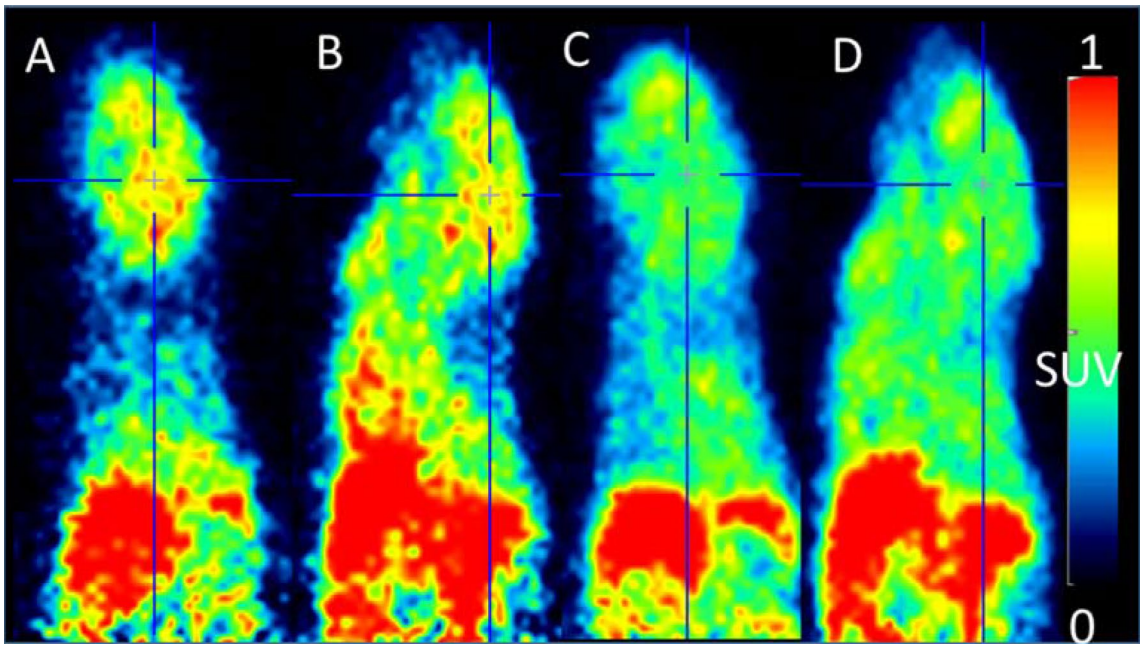

Fig. 3 microPET images of [18F]FMTP in mice, A: 0–10 min summed transaxial; B: 0–10 min summed sagittal; C: 0–40 min summed transaxial; D: 0–40 min summed sagittal. Crosses represent the region with the brain

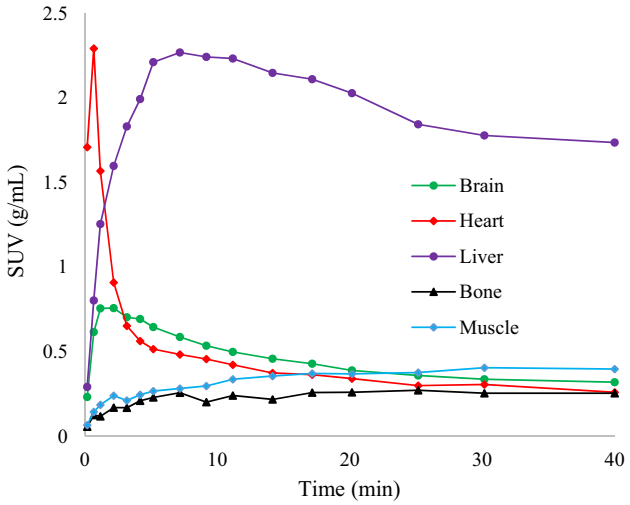

Fig. 4 Representative TACs of [^{18}F]FMTP in mice

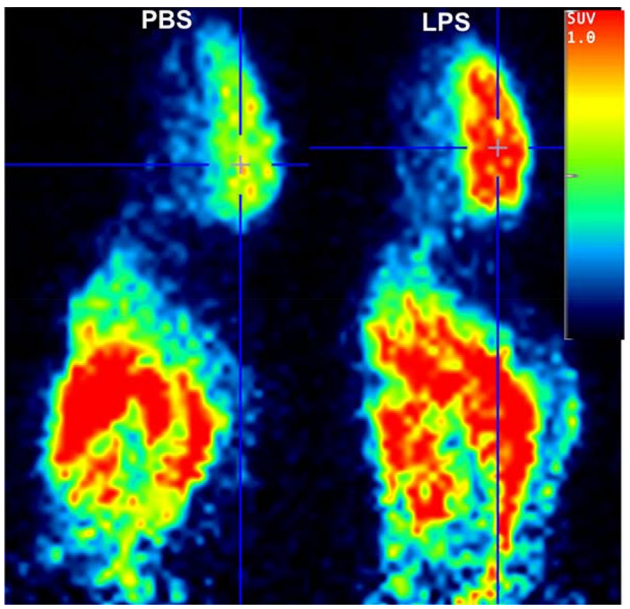

Fig. 5 Representative microPET images of [^{18}F]FMTP in PBS and LPS treated mice

Conclusions

In summary, we report a new method for the radiosynthesis of [^{18}F]FMTP via a chlorine-to-^{18}F-fluorine displacement reaction of aryl[1,3]pyrimidine core molecule. Proof of concept of the use of [^{18}F]FMTP for quantifying COX-2 was established first, in vitro, in COX-2 positive BxPC3 cells. MicroPET imaging of normal mice demonstrated BBB penetration and a fast washout of radioactivity from the brain, likely due to the low concentration of COX-2 in the normal brain.[^{18}F]FMTP showed a higher binding in LPS-induced neuroinflammation compared to binding in the brain of control mice. Specific binding to COX-2 in cell lines, lack of in vivo de-^{18}F-fluorination and skeletal uptake, and BBB permeability, and higher brain binding in neuroinflammation qualifies [^{18}F]FMTP as a potential PET tracer for imaging inflammation where COX-2 overexpression is reported.

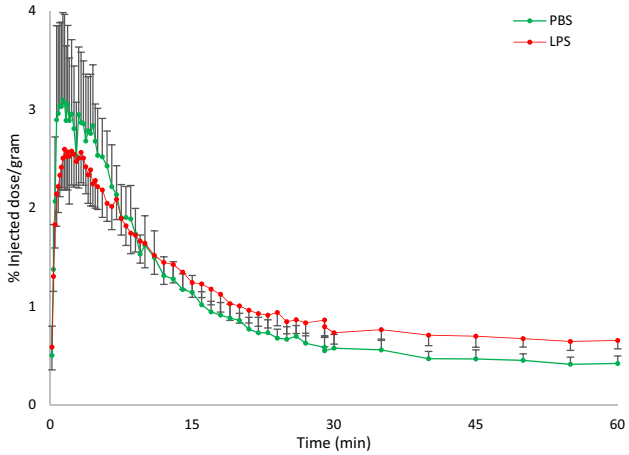

Fig. 6 TACs of [^{18}F]FMTP in PBS and LPS treated mice. Values are reported as the mean ± SD from three independent experiments

Funding This work was funded by Diane Goldberg Foundation (NYSPI/ CUMC) and NCATS UL1TR001873 (Reilly) Irving Institute/ CTSA Translational Therapeutics Accelerator.

Compliance with ethical standards

Conflict of interest Dr. Mann receives royalties for commercial use of the C-SSRS from the Research Foundation for Mental Hygiene. The other authors declare no conflict of interest.

References

1. Fitzpatrick F. Cyclooxygenase enzymes: regulation and function. Curr Pharm Des. 2004;10(6):577–88.
2. DeWitt DL. Prostaglandin endoperoxide synthase: regulation of enzyme expression. Biochim Biophys Acta. 1991;1083(2):121–34.
3. Smith WL, Marnett LJ. Prostaglandin endoperoxide synthase: structure and catalysis. Biochim Biophys Acta. 1991;1083(1):1–17.
4. Ji B, Kumata K, Onoe H, Kaneko H, Zhang M-R, Seki C, et al. Assessment of radioligands for PET imaging of cyclooxygenase-2 in an ischemic neuronal Injury model. Brain Res. 2013;1533:152–62.
5. Yasojima K, Schwab C, McGeer EG, McGeer PL. Distribution of cyclooxygenase-1 and cyclooxygenase-2 mRNAs and proteins in the human brain and peripheral organs. Brain Res. 1999;830(2):226–36.

6. Ho L, Pieroni C, Winger D, Purohit DP, Aisen PS, Pasinetti GM. Regional distribution of cyclooxygenase-2 in the hippocampal formation in Alzheimer's disease. J Neurosci Res. 1999;57(3):295–303.
7. Botting R, Ayoub SS. COX-3 and the mechanism of action of paracetamol/acetaminophen. Prostaglandins Leukot Essent Fatty Acids. 2005;72(2):85–7.
8. Schwab JM, Schluesener HJ, Meyermann R, Serhan CN. COX-3 the enzyme and the concept: steps towards highly specialized pathways and precision therapeutics? Prostaglandins Leukot Essent Fatty Acid. 2003;69(5):339–43.
9. Warner TD, Mitchell JA. Cyclooxygenase-3 (COX-3): filling in the gaps toward a COX continuum? Proc Natl Acad Sci USA. 2002;99(21):13371–3.
10. Choi SH, Aid S, Bosetti F. The distinct roles of cyclooxygenase-1 and -2 in neuroinflammation: implications for translational research. Trends Pharmacol Sci. 2009;30(4):174–81.
11. Minghetti L. Cyclooxygenase-2 (COX-2) in inflammatory and degenerative brain diseases. J Neuropathol Exp Neurol. 2004;63(9):901–10.
12. Guan PP, Wang P. Integrated communications between cyclooxygenase-2 and Alzheimer's disease. FASEB J. 2019;33(1):13–33.
13. Dhir A. An update of cyclooxygenase (COX)-inhibitors in epilepsy disorders. Expert Opin Investig Drugs. 2019;28(2):191–205.
14. Rojas A, Chen D, Ganesh T, Varvel NH, Dingledine R. The COX-2/prostanoid signaling cascades in seizure disorders. Expert Opin Ther Targets. 2019;23(1):1–13.
15. Strauss KI. COX2 inhibitors for acquired brain injuries: is the time ripe? Crit Care Med. 2010;38(2):723–4.
16. de Vries EF, Dierckx RA, Klein HC. Nuclear imaging of inflammation in neurologic and psychiatric disorders. Curr Clin Pharmacol. 2006;1(3):229–42.
17. Fond G, Hamdani N, Kapczinski F, Boukouaci W, Drancourt N, Dargel A, et al. Effectiveness and tolerance of anti-inflammatory drugs' add-on therapy in major mental disorders: a systematic qualitative review. Acta Psychiatr Scand. 2014;129(3):163–79.
18. Na KS, Jung HY, Kim YK. The role of pro-inflammatory cytokines in the neuroinflammation and neurogenesis of schizophrenia. Prog Neuropsychopharmacol Biol Psychiatry. 2014;48:277–86.
19. Mathew ST, Devi GS, Prasanth VV, Vinod B. Efficacy and safety of COX-2 Inhibitors in the clinical management of arthritis: mini review. ISRN Pharmacol. 2011;2011:480291.
20. Yang X, Ma N, Szabolcs MJ, Zhong J, Athan E, Sciacca RR, et al. Upregulation of COX-2 during cardiac allograft rejection. Circulation. 2000;101(4):430–8.
21. Patti R, Gumired K, Reddanna P, Sutton LN, Phillips PC, Reddy CD. Overexpression of cyclooxygenase-2 (COX-2) in human primitive neuroectodermal tumors: effect of celecoxib and rofecoxib. Cancer Lett. 2002;180(1):13–211.
22. Puljak L, Marin A, Vrdoljak D, Markotic F, Utrobicic A, Tugwell P. Celecoxib for osteoarthritis. Cochrane Database Syst Rev. 2017;5:CD009865.
23. Rayar AM, Lagarde N, Ferroud C, Zagury JF, Montes M, Sylla-Iyarreta VM. Update on COX-2 selective inhibitors: chemical classification, side effects and their use in cancers and neuronal diseases. Curr Top Med Chem. 2017;17(26):2935–56.
24. Miao XP, Ouyang Q, Li HY, Wen ZH, Zhang DK, Cui XY. Role of selective cyclooxygenase-2 inhibitors in exacerbation of inflammatory bowel disease: a systematic review and meta-analysis. Current Therapeutic Res. 2008;69(3):181–91.
25. Prabhakaran J, Majo VJ, Simpson NR, Van Heertum RL, Mann JJ, Kumar JSD. Synthesis of [11C]celecoxib: a potential PET probe for imaging COX-2 expression. J Label Comp Radiopharm. 2005;48:887–95.
26. Prabhakaran J, Underwood MD, Parsey RV, Arango V, Majo VJ, Simpson NR, et al. Synthesis and in vivo evaluation of [18F]-4-[5-(4-methylphenyl)-3(trifluoromethyl) -1H-pyrazol-1-yl]benzenesul- fonamide as a PET imaging probe for COX-2 expression. Bioorg Med Chem Lett. 2007;15:1802–7.
27. Toyokuni T, Kumar JSD, Walsh JC, Shapiro A, Talley JJ, Phelps ME, et al. Synthesis of 4-(5-[18F]fluoromethyl-3phenylisoxazol-4-yl)benzenesulfonamide, a new [18F]fluorinated analogue of valdecoxib, as a potential radiotracer for imaging cyclooxygenase-2 with positron emission tomography. Bioorg Med Chem Lett. 2005;15:4699–702.
28. Prabhakaran J, Underwood MU, Zanderigo F, Simpson NR, Cooper AR, Matthew J, et al. Radiosynthesis and in vivo evaluation of [11C]MOV as a PET imaging agent for COX-2. Bioorg Med Chem Let. 2018;28(14):2432–5.
29. Kaur J, Tietz O, Bhardwaj A, Marshall A, Way J, Wuest M, et al. Design, synthesis, and evaluation of an 18F-labeled radiotracer based on celecoxib–NBD for positron emission tomography (PET) imaging of cyclooxygenase-2 (COX-2). Chem Med Chem. 2015;10:1635–40.
30. Wuest F, Kniess T, Bergmann R, Pietszsch J. Synthesis and evaluation in vitro and in vivo of a 11C-labeled cyclooxygenase-2 (COX-2) inhibitor. Bioorg Med Chem. 2008;16:7662–700.
31. De Vries EFJ, van Waarde A, Buursma AR, Vaalburg W. Synthesis and in vivo evaluation of 18F-desbromo-DuP-697 as a PET tracer for cyclooxygenase-2 expression. J Nucl Med. 2003;44:1700–6.
32. De Vries EFJ, Doorduin J, Dierckx RA, van Waarde A. Evaluation of [11C]rofecoxib as PET tracer for cyclooxygenase 2 overexpression in rat models of inflammation. Nucl Med Biol. 2008;35:35–42.
33. Tanaka M, Fujisaka Y, Kawamura K, Ishiwata K, Qinggeletu FY, Mukai T, et al. Radiosynthesis and evaluation of 11C-labeled diaryl-substituted imidazole and indole derivatives for mapping cyclooxygenase-2. Biol Pharm Bull. 2006;29:2087–209.
34. Pacelli A, Greenman J, Cawthorne C, Smith G. Imaging COX-2 expression in cancer using PET/SPECT radioligands: current status and future directions. J Labelled Comp Radiopharm. 2014;57(4):317–22.
35. Tietz O, Marshall A, Wuest M, Wang M, Wuest F. Radiotracers for molecular imaging of cyclooxygenase-2 (COX-2) enzyme. Curr Med Chem. 2013;20(35):4350–69.
36. Kumar JSD, Zanderigo F, Prabhakaran J, Rubin-Falcone H, Parsey RV, Mann JJ. In vivo evaluation of [11C]TMI, a COX-2 selective PET tracer, in baboons. Bioorg Med Chem Lett. 2018;28(23–24):3592–5.
37. Tietz O, Wuest M, Marshall A, Glubrecht D, Hamann I, Wang M, et al. PET imaging of cyclooxygenase-2 (COX-2) in a preclinical colorectal cancer model. Eur J Nuc Med Mol Imag Res. 2016;6(1):37.
38. Tietz O, Marshall A, Bergman C, Wuest M, Wuest F. Impact of structural alterations on the radiopharmacological profile of 18F-labeled pyrimidines as cyclooxygenase-2 (COX-2) imaging agents. Nucl Med Biol. 2018;62–63:9–17.
39. Litchfield M, Wuest M, Glubrecht D, Wuest P. Radiosynthesis and biological evaluation of [18F]Triacoxib: a new radiotracer for PET imaging of COX-2. Mol Pharm. 2020;17(1):251–61.
40. Kim M-J, Shrestha SS, Cortes M, Singh P, Morse C, Liow J-S, et al. Evaluation of two potent and selective PET radioligands to image COX-1 and COX-2 in rhesus monkeys. J Nucl Med. 2018;59(12):1907–12.
41. Gallagher E, Shrestha S, Eldridge M, Cortes M, Yu Z-X, LehmannM, et al. Novel PET radioligands show that COX-2, but not COX-1, is induced by neuroinflammation in rhesus macaque. Biol Psychiatry Ann Meet. 2018;83(9):S160.
42. Prabhakaran J, Kumar JSD, Simpson NR, Kim J, Castrillon J, Molotkov M, et al. Radiosynthesis and evaluation of [18F]FMTP: a potential COX-2 PET ligand. J Nucl Med. 2019;60:1106 **(S-1-)**.

43. Kumar JSD, Mann JJ, Mintz, A, PET Radiolabeled COX-2 inhibitors bearing methysulfonyl arylpyrimidine/isoxazols molecules and uses thereof. U.S. Prov. Appl. No. 62/864, 339; 2019.
44. Cortes-Salva MY, Shrestha S, Singh P, Morse CL, Jenko KJ, Montero Santamaria JA, et al. 2-(4-Methylsulfonylphenyl)pyrimidines as prospective radioligands for imaging cyclooxygenase-2 with PET-synthesis, triage, and radiolabeling. Molecules. 2018;23(11):2850.
45. Orjales A, Mosquera R, López B, Olivera R, Labeaga L, Núñez MT. Novel 2-(4-methylsulfonylphenyl)pyrimidine derivatives as highly potent and specific COX-2 inhibitors. Bioorg Med Chem. 2008;16(5):2183–99.
46. Catorce MN, Gevorkian G. LPS-induced murine neuroinflammation model: main features and suitability for pre-clinical assessment of nutraceuticals. Curr Neuropharmacol. 2016;14(2):155–64.
47. Font-Nieves M, Sans-Fons MG, Gorina R, Bonfill-Teixidor E, Salas-Pérdomo A, Márquez-Kisinousky L, et al. Induction of COX-2 enzyme and down-regulation of COX-1 expression by lipopolysaccharide (LPS) control prostaglandin E2 production in astrocytes. J Biol Chem. 2012;287(9):6454–68.
48. Yao R, Seidel J, Johnson CA, Daube-Witherspoon ME, Green MV, Carson RE. Performance characteristics of the 3-D OSEM algorithm in the reconstruction of small animal PET images Ordered-subsets expectation-maximization. IEEE Trans Med Imag. 2000;19:798–804.
49. Yang Z, Zan Y, Zheng X, Hai W, Chen K, Huang Q, Xu Y, Peng J. Dynamic FDG-PET imaging to differentiate malignancies from inflammation in subcutaneous and in situ mouse model for non-small cell lung carcinoma (NSCLC). PLoS ONE. 2015;10(9):e0139089.